

Production of nanostructured crystalline composite using residual ashes from flocculated sludge burning process in a poultry slaughterhouse wastewater treatment system

L. E. N. Castro^{1}, L. R. Matheus¹, L. J. C. Albuquerque², L. J. Gasparini³,
K. C. Fagnani³, H. J. Alves³, L. M. S. Colpini¹*

¹Universidade Federal do Paraná, Jandaia do Sul, PR, Brazil

²Universidade Federal do ABC, Santo André, SP, Brazil

³Universidade Federal do Paraná, Palotina, PR, Brazil

Abstract

Nanostructured crystalline composite (activated carbon) was synthesized from residual ashes of the burning process of the sludge generated in the flotation step of a poultry slaughterhouse and was used for Allura red dye adsorption. The ashes were chemically activated using two types of reagents, H_2O_2 and H_3PO_4 , and the structure, morphology, and surface of the adsorbents were characterized by different techniques such as scanning electron microscopy with energy dispersive spectroscopy (SEM/EDS), N_2 adsorption/desorption isotherms with Brunauer-Emmett-Teller (BET) method and Barret-Joyner-Hallenda (BJH) method, Fourier transform infrared spectroscopy (MID/FTIR), X-ray diffraction (XRD), and the point of zero charge (PZC). The adsorbent synthesized with H_3PO_4 at 400 °C displayed the best performance in removing dye molecules in 10 mg.L⁻¹ solution, with a removal rate of approximately 100% when using a concentration of 2 g.L⁻¹ in particle size of 0.42 mm. Besides that, the adsorbent synthesized with H_3PO_4 had a particle diameter of approximately 15 Å, a size corresponding to the nanometer range, presented a crystallinity structure with well-defined phases such as quartz and the major elements in the composition were carbon and silicon. The surface area of the ashes enlarged from 14.71 to 448.1 m².g⁻¹ when H_3PO_4 was used as an activator, producing a high-quality adsorbent, with an excellent cost-benefit, being it possible to be produced for a price of 9.35 USD.kg⁻¹, a price lower than the commercial activated carbon, making it a promising candidate for application in an industrial environment.

Keywords: adsorbents, activated carbon, phosphoric acid, hydrogen peroxide, Allura red AC, food waste.


INTRODUCTION

Residual ashes are produced by the process of burning fuel in boilers during the burning process; the produced ash that falls onto the bottom of the boiler, known as the ashtray, is classified as bottom ash, and part of the ash produced is also carried by air and ends up trapped in the boiler filters, which is classified as fly ash [1, 2]. Between 2017 and 2018, countries such as India, China, United States, and Germany produced around 350 million tons of residual ash, with an estimated 700 million tons worldwide [1, 3]. These residual ashes from the burning process are usually used on an industrial scale to make construction materials like Portland cement and/or refractory bricks, but the unused parts of this waste end up being stored in an area of the industry or disposed of as garbage, which can lead to soil degradation and pose a risk to groundwater bodies [4-6]. To avoid this risk, the use of these residual ashes for the synthesis of zeolitic material has been studied in the literature [7, 8]. However, due to the high expense of the process and the difficulties of creating a material with a well-defined structure, this application has received little attention [9, 10].

Alternative uses for these ashes include the creation of adsorbent materials, particularly activated carbons or carbon

nanostructures, which are produced at a low cost and have ideal properties to produce an adsorbent material [11, 12]. Overall, residual ashes contain the properties needed to be an effective adsorbent, such as a high concentration of minerals, particularly carbon, silicon, and aluminum, and high volatile content, which aids in the formation of a rich pore structure [13, 14]. This indicates that the base material, a residue, can be easily converted into an adsorbent material, extremely efficient and low-cost [15]. This adsorbent material must be activated before its use and one of the methods is the chemical activation with nitric acid, phosphoric acid, potassium hydroxide, and/or potassium carbonate, or physical activation with steam, carbon dioxide, ozone, and other procedures and techniques can be used to activate carbon-based materials [16-22]. Some factors, such as the cost and time spent synthesizing the material, the required equipment, the degree of difficulty of the synthesis, the type of reagent used and its toxicity, and, most importantly, the characteristics of the material produced, must be considered before selecting an activation method [13, 23]. Considering these factors, chemical activation emerges as a promising option, since it produces materials with a high micropore content and large surface area, which can be employed for the adsorption of high molecular weight species like azo dyes. Furthermore, most reagents are non-toxic, and activation takes place in a short reaction time and at a low temperature of 300-400 °C, optimizing this process while lowering energy and personnel expenses. Furthermore, the

*luz_nc@yahoo.com

 <https://orcid.org/0000-0002-5968-8968>

reagents required are frequently inexpensive, reducing the overall cost of the operation [13, 19, 24-26], and promoting a more quick and more effective way of treating these effluents, contrary to the conventional methods [26].

Primary treatments, including coagulation, flocculation, and sedimentation, are commonly employed to treat liquid industrial effluents and are part of the conventional methods for wastewater treatment. These treatments are well-known and well-studied in the literature [11, 27, 28]. However, they require large building areas, are used to treat large volumes of effluent, and as a result, use a lot of material to treat the effluent and generate a great deal of sludge that needs to be treated again [29-31]. Moreover, they are frequently unable to remove the molecules responsible for the effluents' color, such as dye molecules, necessitating further treatment processes, increasing the process's time and expense [32, 33]. Therefore, the adsorption process presents itself as a method that is efficient, simple to operate, low in operational cost, has zero sludge production, no chemical requirement, and is extremely competent in discoloration and degradation processes, in addition to being able to reuse the industrial waste in the form of activated carbon [32, 34, 35]. One of this industrial waste is the sludge produced during the flocculation stage in the treatment of poultry slaughterhouse wastewater; this residue contains substantial amounts of total organic carbon, chemical oxygen demand, total solids, nitrogen, and phosphorus, making them very dangerous and harmful to the environment; besides that, the cost to treat this sludge surpass values of USD 15000 per year depending on the size of the wastewater treatment plant [27]. In this way, the use of this residue for the production of materials with high added value, such as adsorbents, shows itself as a trendy and efficient alternative, which can be applied in the adsorption processes of other liquid residues, particularly in the food industry, which has been studied in the recent literature, showing results that are generally better than other processes, making activated carbon adsorption using residues as base material an emerging technology that the industry may begin to adopt for the treatment of its liquid waste [11, 32, 36]. Thus, the aim of this study was the synthesis and characterization of nanostructured crystalline composite (activated carbon) obtained from residual ashes of the burning process of the sludge generated in the flotation step of a poultry slaughterhouse and evaluation of the application in adsorptive processes of Allura red food dye.

MATERIALS AND METHODS

Raw material preparation: the material used for the preparation of the adsorbents came from the flocculation stage of the effluent treatment process of a poultry slaughterhouse in the western region of Paraná, Brazil, where the sludge generated in the flotation system was dehydrated in a Tricanter and the material generated was burned mixed with wood chips in the boiler. The residue generated by the burning process, ashes, were used as raw material to produce the adsorbents. The process of obtaining

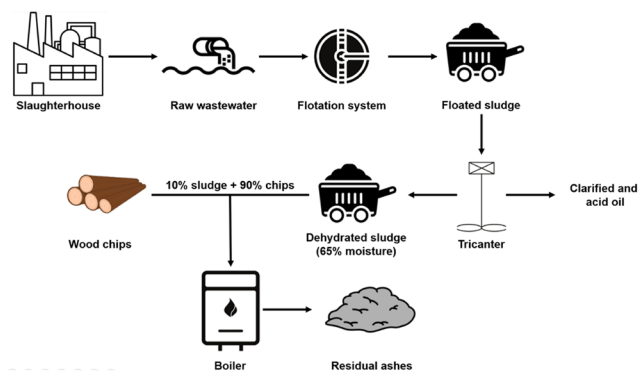


Figure 1: Scheme for obtaining the ash used in the production of the adsorbents.

the ashes is shown in Fig. 1.

Adsorbent preparation: the sludge-burning residue (ashes) was chemically activated using two methods to obtain the activated carbon: a) activation with hydrogen peroxide (H_2O_2), and b) phosphoric acid (H_3PO_4); in addition to evaluating the effect of chemical activation on the adsorbent properties, the effects of the thermal activation step (carbonization) on the synthesis of materials were also evaluated; a scheme with the synthesis steps is shown in Fig. 2. The activation using H_2O_2 was adapted from Gao *et al.* [37]; first, 30 g of ashes were mixed with H_2O_2 solution (Nuclear, 30% purity, 30% w/v) in a proportion of 1:3 (w/v) in an ultrasonic bath for 30 min and then heated at 80 °C for 5 h. Then, the material was washed with distilled water to remove the excess peroxide and dried at 110 °C for 12 h. Then, the sample was carbonized at 400 °C for 3 h with a heating rate of 10 °C.min⁻¹. The activation using H_3PO_4 was adapted from Han *et al.* [38] and Patnukao and Pavasant [39]; first, 30 g of ashes were mixed with H_3PO_4 solution (Nuclear, 85% purity, 85% w/v) in a proportion of 1:1 (w/v); then the mixture was agitated for 15 min and left to rest for 12 h to complete the impregnation of the material. Then, the material was washed with approximately 100 mL of distilled water to remove the excess acid and dried at 80 °C for 8 h. Then, the sample was carbonized at 400 °C for 3 h with a heating rate of 10 °C.min⁻¹. In the end, the sample was washed with $NaHCO_3$ (Nuclear, 99% purity, 2% w/v) until pH=7 was reached; to remove excess water, the sample was dried in an oven at 120 °C for approximately 6 h or until complete drying. The adsorbents obtained were stored in vacuum packages at room temperature and labeled according to Table I.

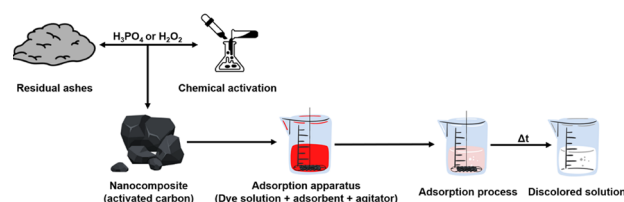


Figure 2: Scheme for obtaining the nanocomposite and the adsorption apparatus.

Table I - Sample coding based on the activation type.

Sample	Chemical activation		Thermal activation
	H ₂ O ₂	H ₃ PO ₄	
Ashes	Not activated and not carbonized		
A.C. (I)	x	Absent	Absent
A.C. (II)	x	Absent	x
A.C. (III)	Absent	x	Absent
A.C. (IV)	Absent	x	x

Adsorbent characterization: the morphology was observed on scanning electron microscopy with energy dispersive spectroscopy (SEM/EDS, Vega3, Tescan) using double-sided carbon tape to fix the sample, which was metalized with a thin layer of gold on the surface (5 nm, 35 mA). The N₂ adsorption/desorption isotherms were measured on a sorption analyzer (Nova 2000e, Quantachrome Instruments) at -196 °C after vacuum activation at 150 °C for 3 h. The surface area, pore volume, and pore diameter were calculated from the Brunauer-Emmett-Teller (BET) method, and pore size distributions were calculated with the Barret-Joyner-Hallenda (BJH) method. The materials structures were studied by Fourier transform infrared spectroscopy (FTIR, Spectrum Two, Perkin Elmer) measuring transmittance from 400-4000 cm⁻¹ and X-ray diffraction (XRD, Stadi-P powder diffractometer, Stoe) with Rietveld refinement. The surface charge distribution was determined by the point of zero charge (PZC) using the 'experiment of 11 points' method [11].

Adsorption experiments. Preliminary tests: preliminary adsorption assays were performed to evaluate the adsorptive capacity of the materials in the removal of Allura red AC dye (Duas Rodas, 85% purity) in aqueous solutions, varying

some parameters such as activation method, particle size, pH of the reaction medium, and concentration of the adsorbent; the apparatus is shown in Fig. 2. In the activation method test, the effect of the different methods of activation on the adsorptive capacity of the materials was evaluated; the adsorbent concentration was 1 g.L⁻¹, dye concentration at 10 mg.L⁻¹, pH of the solution at 6.81, and reaction time of 12 h; these parameters remained constant during all tests. With the material that obtained the highest percentage of removal of the dye in solution during the test of the activation methods, a granulometric test was carried out to evaluate the effect of the different particle sizes on the adsorptive performance of the materials, the particle diameter evaluated varied between 0.088-0.168 mm and the bottom of the sieve set (dp<0.088 mm). With the adsorbent that performed better in the previous tests, the impact of the dye solution pH on the performance of the adsorbents was evaluated; the test parameters were kept the same as the previous ones, but the pH of the solution was varied from 2 to 12, with HCl (Dinâmica, 37% purity, 0.1 mol.L⁻¹) and NaOH (Dinâmica, 97% purity, 0.1 mol.L⁻¹) solutions. Finally, with the other parameters determined, the concentration of the adsorbent was varied to find which value would have the greatest significance in removing the dye from the solution, so the concentration was varied between 0.5 and 10 g.L⁻¹. All tests were performed in an orbital shaker (TE-4200, Tecnal) at a room temperature of 25 °C. The adsorptive capacity of the material was evaluated by removing the dye molecules present in the solution by the adsorbent according to Eq. A, using a UV spectrophotometer (EEQ-9006, Astral Scientific) at the maximum wavelength of the dye at 504 nm:

$$R = \frac{C_0 - C}{C_0} \cdot 100 \quad (A)$$

Table II - Control variables considered in 2² factorial design and experiments.

Variable	Axial point (-√2)	Low level (-1)	Central point (0)	High level (+1)	Axial point (+√2)
Dye concentration (mg.L ⁻¹)	2	10	30	50	58
Reaction temperature (°C)	16	20	30	40	44
Assay	Dye concentration (mg.L ⁻¹)		Reaction temperature (°C)		
1	10		20		
2	10		40		
3	50		20		
4	50		40		
5	2		30		
6	58		30		
7	30		16		
8	30		44		
9	30		30		
10	30		30		

where R (%) is the percentage of removal of the Allura red dye from the solution by the adsorbent, C_0 ($\text{mg}\cdot\text{L}^{-1}$) is the initial concentration, and C ($\text{mg}\cdot\text{L}^{-1}$) is the final solution concentration.

Batch tests: after the preliminary tests, the parameters evaluated that obtained the best adsorptive performance were adopted for batch tests. To maximize even more the removal of the Allura red dye from the aqueous solution, a 2^2 complete factorial design was carried out to assess the influence of the parameter inherent to the solution on the adsorptive capacity of the activated carbons. The variables studied are shown in Table II. The experiments were carried out in an orbital shaker (TE-4200, Tecnal) and the removal of the dye molecules by the adsorbent present in the solution was assessed according to Eq. A and the results were submitted for statistical analysis.

Cost analysis: a cost analysis of the adsorbent synthesis was performed, based on the methodology of the Association for the Advancement of Cost Engineering. Assumptions for scaled-up production cost comparisons were made from the information presented in this study and considering only the processing of residual ash to activated carbon.

Statistical analysis: the results were expressed as mean \pm standard deviation. The factorial design statistical analysis was performed to assess the effect of factors under the response variable and the interaction was tested statically by ANOVA at a significance level of 0.05. In addition, the response variable was optimized using the simplex method.

RESULTS AND DISCUSSION

Adsorbent characterization

Fig. 3 shows the SEM images obtained for the adsorbents; it was possible to observe that all materials presented a ragged surface with granular and laminar particles; these characteristics are common for this type of biosorbents [11, 40]. The ashes and A.C. (III) and (IV) showed a high distribution of pores on the surface; this is a common characteristic of materials that have an excellent adsorptive capacity, as reported previously [38-41]. However, the A.C. (I) and (II) did not show a significant number of pores on their surface, probably due to the type of treatment that the materials were submitted [42, 43]. The EDS analysis allowed us to determine the elemental composition of the adsorbents and the results are shown in Table III. In general, oxygen was the major element in the adsorbent's compositions; this was because the materials were submitted to a carbonization process in the presence of air. The A.C. (III) and (IV) presented the highest levels of carbon; usually, good adsorbent materials have a high amount of carbon in their composition [11, 44]. Other elements were present such as aluminum, silicon, potassium, calcium, and iron, which came from the nature of the base material, in this case, the sludge from the coagulation process [11]. Finally, the phosphorus present in the composition of the adsorbents A.C. (III) and (IV) came from the synthesis process that used phosphoric acid (H_3PO_4) as a synthesis reagent.

Fig. 4 shows the N_2 adsorption-desorption experiments for the adsorbents used in the assays and Table IV shows the summarized parameters. It was possible to observe (Fig. 4a) that all the isotherms resembled the type I isotherm [45], a typical characteristic of microporous materials (<20 Å); also, some of these isotherms may have a wider range for pore size distributions including wider micropores and possibly narrow mesopores ($<\sim 25$ Å) [46-48]. When Fig. 4a was analyzed, it was possible to see that the N_2 adsorption started to grow in the low levels of p/p_0 , but as the p/p_0 value increased, there was no pretty gain in the volume of N_2 adsorbed. This showed that adsorbents had a high micropore structure. Besides, no hysteresis loop was observed in the adsorption-desorption of the adsorbents; this indicated that mesopores of adsorbents were at a quite low number or none [26]. Pore size distributions (PSDs) for adsorbents were calculated with the Barret-Joyner-Hallenda (BJH) method [49], using N_2 adsorption branches with results illustrated in Fig. 4b. As observed, all adsorbents exhibited a distribution of pores no larger than 20 Å with most pores in the range of micropores. The PSD curves for all the materials indicated that micropores constituted the main structures with slightly small-sized mesopores in the A.C. (II).

It was possible to observe from Table IV that the surface area of the ashes after being treated with the activating agents was reduced, from 14.71 to 10.81 $\text{m}^2\cdot\text{g}^{-1}$ using H_2O_2 [A.C. (I)] and 11.07 $\text{m}^2\cdot\text{g}^{-1}$ using H_3PO_4 [A.C. (III)]. This can be explained once the solvents can permeate the entire structure of the material promoting clogging of the pores, agglutination of the material, and a decrease in the volume of the pores, which makes the gas that travels through the surface of the adsorbent find it difficult to sweep the entire area and consequently report a decrease in the value of the specific surface area. This decrease in the surface area of the adsorbents causes them to have their adsorption activity reduced, in addition to promoting an enlargement in the pore diameter changing the microporous structure of the material. However, when looking at the materials that were chemical activated and calcined, there was a significant increase in the value of their surface area, from 14.71 to 94.22 $\text{m}^2\cdot\text{g}^{-1}$ for the A.C. (II) and 448.10 $\text{m}^2\cdot\text{g}^{-1}$ for the A.C. (IV). This behavior came from the combination of both chemical and thermal activation; usually, activation techniques tend to improve the inherent characteristics of the base materials, such as their surface area; this occurs since the reagents during chemical activation manage to percolate the structure of the material and impregnate in pre-existing sites; when proceeding with thermal activation, the heat of the reaction causes these reagents to volatilize and leave 'paths' that form a porous structure when leaving the material structure. In general, materials with a high number of pores on the surface tend to have a high surface area, which explains the behavior observed for A.C. (II) and (IV) adsorbents. Several studies in the literature reported behavior similar to those observed for the adsorbents in question. Table V shows the results of surface area for adsorbents before and after activation obtained by other authors.

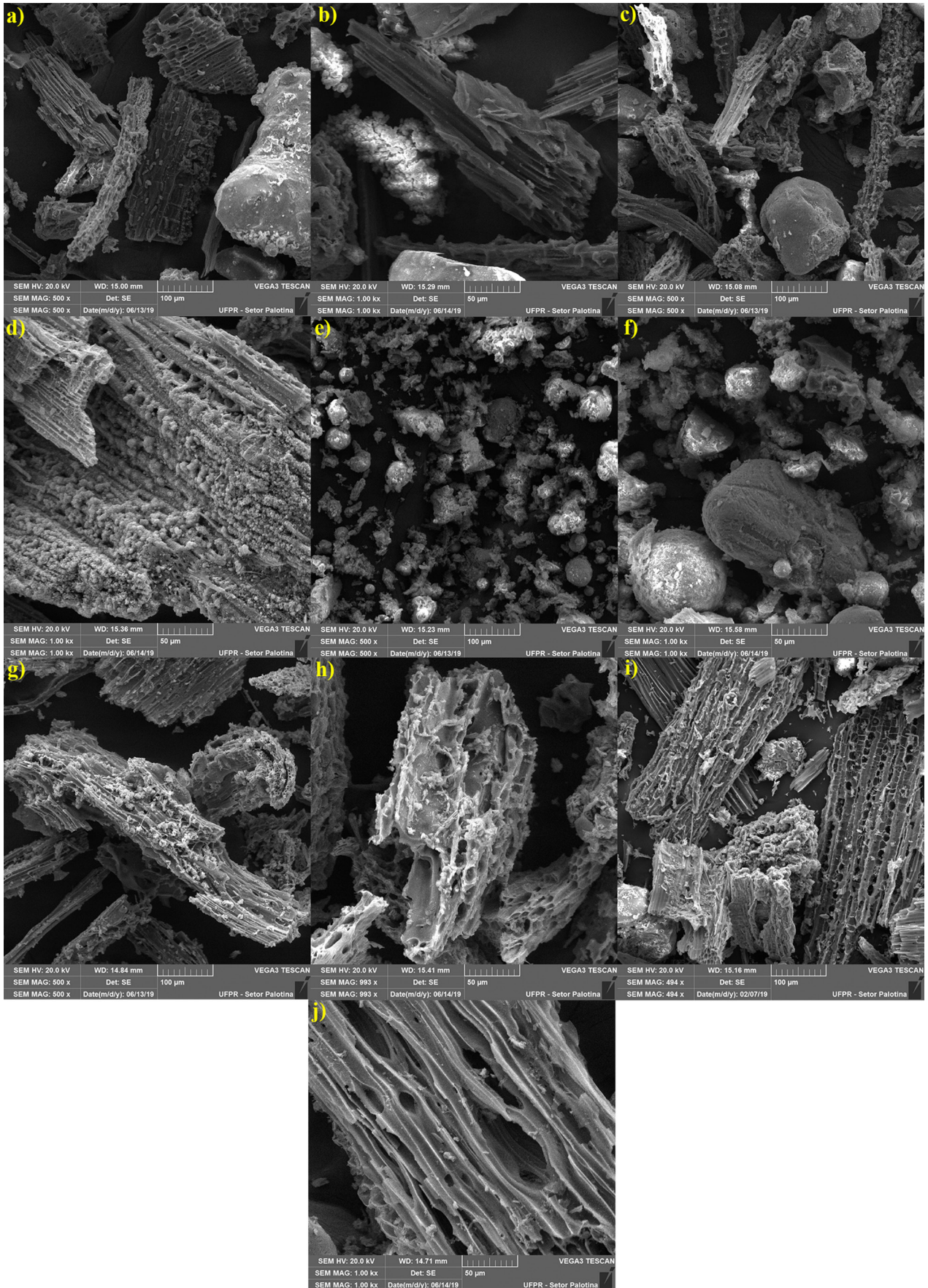


Figure 3: SEM images for the adsorbents: a,b) ashes; c,d) A.C. (I); e,f) A.C. (II); g,h) A.C. (III); and i,j) A.C. (IV).

Table III - Results of EDS analysis.

Adsorbent	C (wt%)	O (wt%)	Al (wt%)	Si (wt%)	K (wt%)	Ca (wt%)	Fe (wt%)	P (wt%)
Ashes	3.86	49.17	4.95	26.45	7.06	3.48	5.03	-
A.C. (I)	4.86	52.46	0.38	24.60	3.10	14.23	0.37	-
A.C. (II)	8.73	54.57	1.40	16.54	0.75	16.52	1.49	-
A.C. (III)	57.46	16.20	0.32	12.97	0.75	2.21	3.22	6.87
A.C. (IV)	63.47	7.61	0.18	11.37	1.65	4.22	2.79	8.71

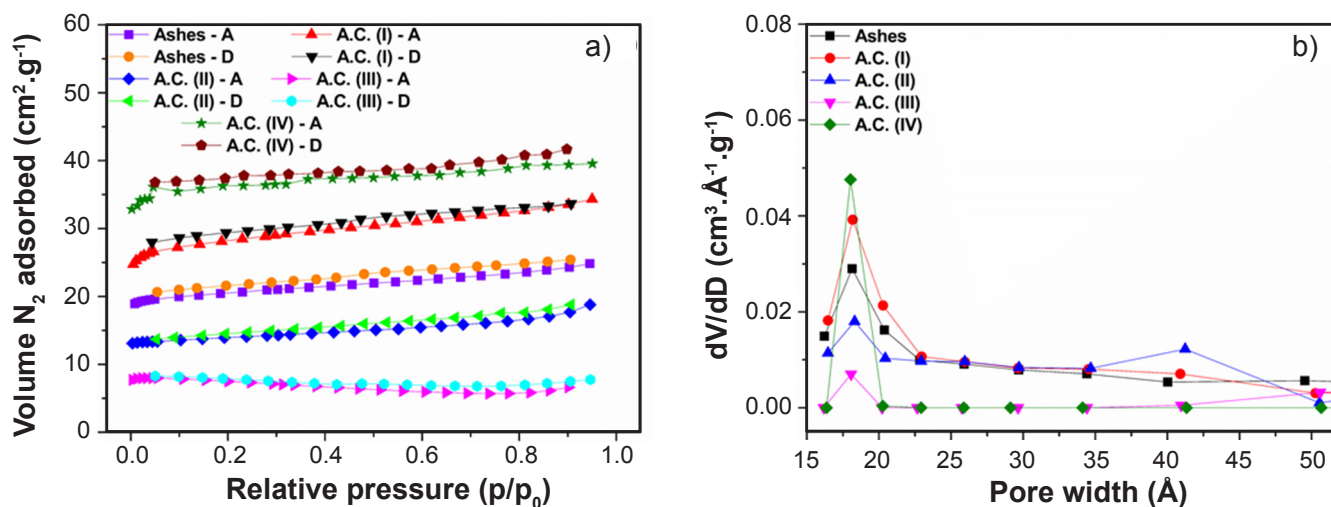
Figure 4: N_2 adsorption-desorption isotherms (a) and pore size distribution for the adsorbents (b).

Table IV - Textural properties of the adsorbents.

Adsorbent	S_o ($m^2.g^{-1}$)	V_p ($10^{-3} cm^3.g^{-1}$)	d_p (Å)
Ashes	14.71	13.40	17.90
A.C. (I)	10.81	9.40	20.70
A.C. (II)	94.22	25.50	15.00
A.C. (III)	11.07	1.40	21.50
A.C. (IV)	448.10	91.80	14.70

S_o : specific surface area; V_p : pore volume; d_p : pore diameter.

In Fig. 5 the FTIR spectra for the adsorbents are shown, to verify the presence of functional groups that can act as adsorption sites for the material. The spectra were divided into four regions with representative peaks in all samples but indicated only once in the figure, where there were expressive bands between 3125 and 2750 cm^{-1} (1st region) with peaks at 2980, 2920, and 2850 cm^{-1} , which are characteristics of the C-H aliphatic stretching vibration of alkane and alkene groups of the adsorbents [53, 54]. In the second region, there were bands between 2375 and 1875 cm^{-1} with a peak at 2325 cm^{-1} , which is characteristic of the $C\equiv C$ stretching vibration of alkyne groups; also, the peak at 2156 cm^{-1} represents the $C=C$ vibration in the ring structure and the peak at 2004 cm^{-1} is characteristic of $C=C=C$ vibration of allene groups of the adsorbents [55-57]. The third region had bands between 1875 and 1250 cm^{-1} with a representative peak at 1750 cm^{-1} , which

is characteristic of the vibration of C-O and C=O groups, and a peak at 1410 cm^{-1} corresponding to the C-C stretch in the aromatic group present in the activated carbon's structure [55, 58]. Finally, the fourth region had bands between 1250 and 750 cm^{-1} and showed a peak at 1080 cm^{-1} characteristic of Si-O-C and Si-O-Si structures, also the peaks at 1065 and 956 cm^{-1} , which represented phosphorous species (P-O-P and/or P^+-O^-) symmetrical vibrations, the peak at 1000 cm^{-1} related to the C-O stretching vibration of alcohols, carboxylic acids, esters, ethers and others species on the surface of the adsorbents, finally the peaks at 874 and 830 cm^{-1} characteristics of the C-H bending vibration, which are common of carbonaceous species such as activated carbons [53, 58-61].

Fig. 6 shows the XRD patterns for the adsorbents obtained, intending to verify if there was the formation of the crystalline structure of the composite. The peaks found at 20.85°, 26.63°, 36.53°, 39.46°, 40.27°, 42.43°, 45.77°, 50.12°, 54.85°, 55.33°, 59.93°, 67.71°, 68.28°, 73.47°, 75.62°, and 79.85° were all related to the quartz phase (hexagonal) of SiO_2 , according to JCPDS file 86-1560. However, the peak found at 29.40° was related to the calcite phase (rhombohedral) of $CaCO_3$, according to JCPDS file 83-1762. Yet, the peaks found at 32.30°, 37.47°, and 54.03° were related to the lime phase (cubic) of CaO , according to JCPDS file 82-1691. Finally, the peaks found at 22.88° and 24.11° were related to the pseudo-cristobalite phase (tetragonal) of SiO_2 and a silicon phosphate oxide (SiP_2O_7).

Table V - Comparison of literature results for the surface area of activated carbons.

Precursor	BET surface area (m ² .g ⁻¹)	Chemical activator	Activation temperature (°C)	Ref.
Poultry slaughterhouse wastewater treatment sludge	14.71	-	-	This study
Beverage wastewater treatment sludge	448.1	H ₃ PO ₄	400	
Sewage sludge	78.00	-	-	[50]
	642.0	ZnCl ₂	800	
Dried cassava sludge	253.8	-	-	[51]
	680.3	KOH	500	
Dried cassava sludge	0.750	-	-	[52]
	509.0	ZnCl ₂	500	

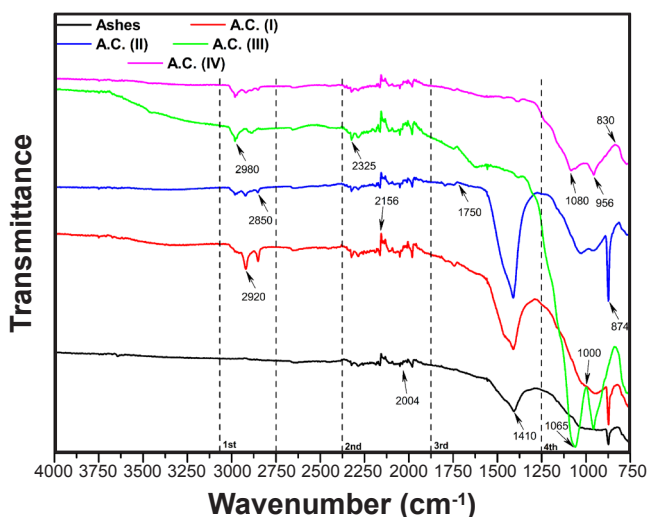


Figure 5: FTIR spectra of the adsorbents.

tetragonal phase, according to the JCPDS files 82-1556 and 22-1320, respectively [62]. It was also possible to observe in Fig. 6, a tendency of crystalline phase change between the ashes and the synthesized adsorbents; in the ashes' X-ray diffractogram, it was possible to identify phases related to the calcium element, such as calcium oxide and calcium carbonate, but the activated materials, whether chemically or thermally treated, had their crystal structure altered as can be seen in the other diffractograms, where there was a tendency to change in the profile of the peaks. In the A.C. (IV) diffractogram, for example, no phase other than quartz was detected, indicating that the unit cell of the crystal lattice of this material was composed basically of the elements silicon and oxygen in a hexagonal arrangement. This change most likely came from the chemical activation with phosphoric acid and heat treatment that this material was subjected to; in fact, the intention of activating an adsorbent is to change its structure to provide the formation of a porous surface with high adsorbent capacity; the fact that the base material was rich in silicon allowed all materials to show peaks related to the silicon oxide phases, a material that is highly known in the literature for being a material with a rich porous structure

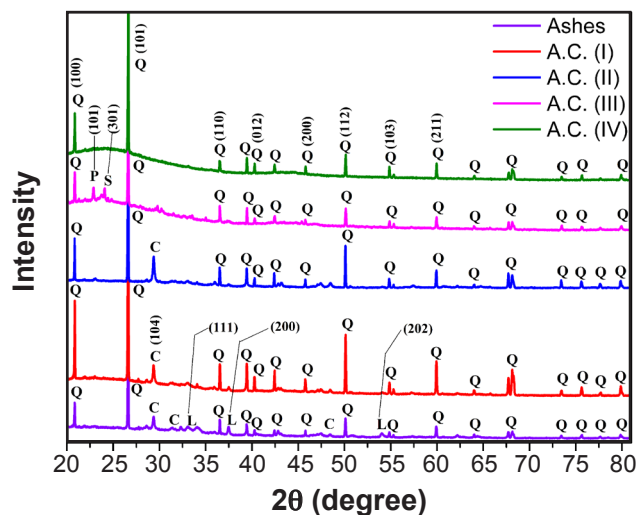


Figure 6: X-ray diffraction patterns of the adsorbents. Q: quartz (SiO₂), P: pseudo-cristobalite (SiO₂), S: silicon phosphate (SiP₂O₇), C: calcite (CaCO₃), L: lime (CaO). The numbers in parentheses indicate the crystallographic plane.

and high adsorptive capacity [26, 44, 63].

Table VI presents the results of the phase composition of the materials obtained through the Rietveld refinement and the adapted Spurr equation by [64]:

$$Z = \frac{I_x}{I_x + 1.26 I_y} \cdot 100 \quad (B)$$

where Z (%) was the content of the phase in the diffractogram, I_x (a.u.) the intensity of the highest peak value of the diffractogram, I_y (a.u.) the peak intensity of the phase of interest with the highest intensity value on the diffractogram. In general, the quartz (SiO₂) was the major phase in all adsorbent materials with a content >64% for both the Rietveld refinement and the Spurr equation. This result corroborated that obtained in the elemental analysis of the EDS (Table III) and in the infrared spectra (Fig. 5) that indicated the presence of silicon in the composition of the

Table VI - Phase composition of the adsorbents.

Adsorbent	Oxide	Phase	Rietveld refinement (%)	Spurr equation (%)	RMSE
Ashes	SiO ₂	Quartz	66.40	64.52	1.330
	CaCO ₃	Calcite	26.10	27.12	
	CaO	Lime	7.50	8.36	
A.C. (I)	SiO ₂	Quartz	83.24	81.98	1.260
	CaCO ₃	Calcite	16.76	18.02	
A.C. (II)	SiO ₂	Quartz	78.80	78.10	0.700
	CaCO ₃	Calcite	21.20	21.90	
A.C. (III)	SiO ₂	Quartz	79.30	83.74	3.140
	SiO ₂	Pseudo-cristobalite	12.59	10.35	
	SiP ₂ O ₇	Silicon phosphate	8.11	5.91	
A.C. (IV)	SiO ₂	Quartz	100	100	-

RMSE: root-mean-square error.

adsorbents, in addition to the presence of phases related to the calcium element, such as calcium carbonate and calcium oxide. Furthermore, it was possible to observe that the experimental results obtained by the Spurr equation were very close to those theoretically obtained by the Rietveld refinement (RMSE<3.14); this showed that the refinement was accurate in determining the composition of crystalline phases in the synthesized materials. The change in the format of the diffractograms (Fig. 6) was confirmed by the refinement data; it was possible to note that the amount of quartz phase increased in all activated carbons synthesized from ashes, especially the A.C. (IV) in which its composition was 100% quartz; this is relevant data that showed that this material can be used as a source of crystalline SiO₂ in various processes from catalyst synthesis, molecular sieves, and zeolites, in addition to being used in energy applications and civil construction [65-68].

The results of the PZC analysis are shown in Fig. 7 and Table VII; Allura red dye solution had a pH=6.81 at a concentration of 10 mg.L⁻¹. The point of zero charge evaluates the adsorbent's surface behavior; it may suggest the predisposition of a material's surface as to its basicity or acidity, representing that the material is negatively charged when the pH_{PZC} is higher than the pH of the solution, and positively charged when the pH_{PZC} is lower than the pH of the solution [11]. Fig. 7 shows that the adsorbent had different values of pH_{PZC}, resulting in different surface charges. For ashes, A.C. (I) and (II) the pH_{PZC} was higher than the pH of the solution, indicating that the adsorbents' surfaces were negatively charged, causing cations to be adsorbed to the surface to balance the negative charges. Differently, the pH_{PZC} of the other activated carbon [A.C. (IV)] was lower than the pH of the solution, indicating that the surface was positively charged and attracted negatively charged species; dye molecules are known to have free electrons in their structure, so they tend to have a negative charge, aiding the adsorption process [69, 70].

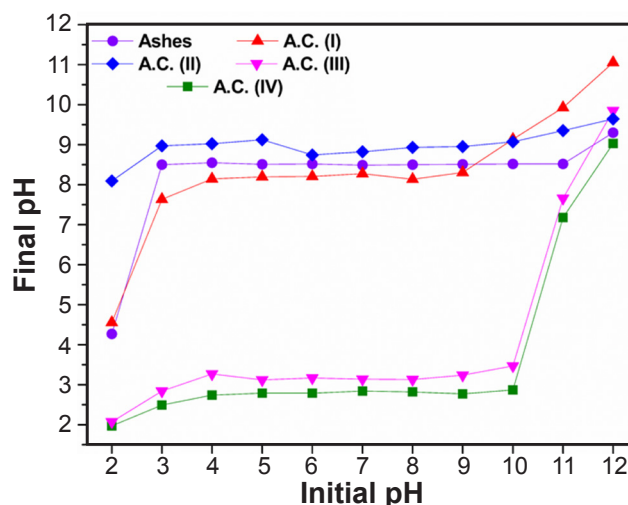


Figure 7: Graph of PZC results for the adsorbents.

Table VII - pH_{PZC} (pH at point of zero charge) for the adsorbents.

Ashes	A.C. (I)	A.C. (II)	A.C. (III)	A.C. (IV)
8.51	8.44	8.98	3.22	2.76

Preliminary adsorption tests

Fig. 8 shows the results of the preliminary tests. It was possible to observe that the activation method had an influence on the removal value of Allura red dye from the solution (Fig. 8a). A.C. (IV) was the sample that had the highest removal value, approximately 47%. This excellent performance was due to the material's properties, which included a large surface area, a large pore distribution, and a positive surface charge; all of these characteristics made the material an excellent adsorbent. However, the other materials presented unsatisfactory results, with less than 35% of Allura red dye removal. A.C. (I) had the lowest removal value, approximately 15%. This low discoloration

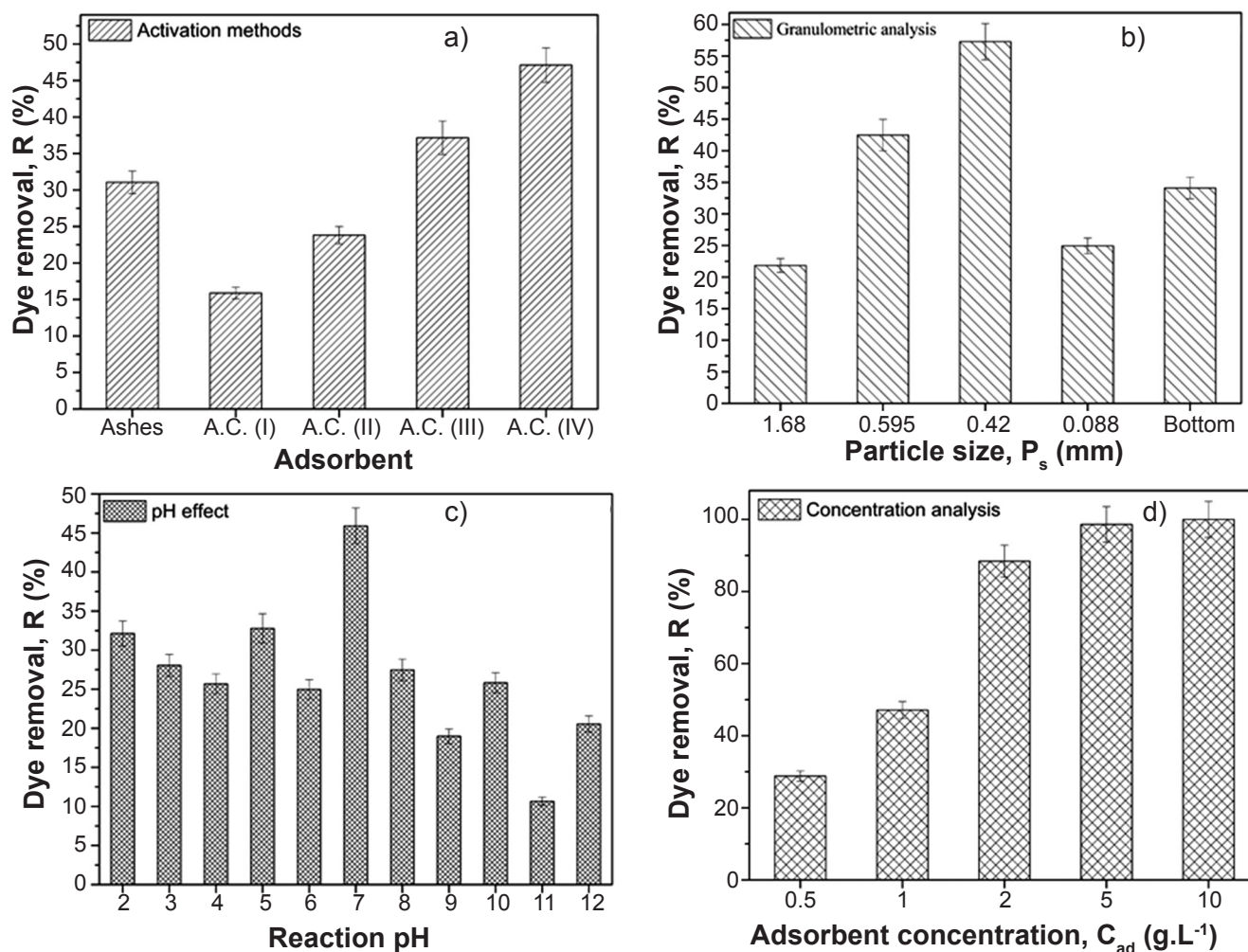


Figure 8: Results of preliminary tests for the adsorption of Allura red dye showing the effects of: a) activation method; b) particle size; c) reaction pH; and d) adsorbent concentration (parameters: $C_{\text{dye}}=10 \text{ mg.L}^{-1}$, $t_{\text{rea}}=12 \text{ h}$, $V_{\text{dye}}=50 \text{ mL}$, $T_{\text{rea}}=25 \text{ }^{\circ}\text{C}$).

rate was attributed to the surface charge of these materials, which exhibited a charge equal to the affluent, causing the charges to be repelled and, as a result, hampering the adsorptive process, despite the presence of micropores on the structure. It is noteworthy that the thermal activation also wielded a positive influence on the removal of the dye from the solutions; when we observed the adsorbents treated with hydrogen peroxide, A.C. (I) and (II), there was a clear increase in the removal of the Allura red dye between the adsorbents I and II, where material II was thermally activated promoting approximately 50% greater removal. The same was observed for the materials activated with phosphoric acid, A.C. (III) and (IV), in which the adsorbent IV that was thermally activated obtained a higher removal than the material not heat treated. In general, this behavior was expected, since the heat promoted during the carbonization step tends to generate gas vapor inside the structure, produced from the evaporation of the solvents used in the synthesis. When escaping to the environment, this gas tends to create 'pathways' rich in micro and mesopores, that is responsible for assisting in the adsorption process. Besides, heat helps

to increase the surface area of the material and promote active sites, both essential characteristics for the adsorptive process. Thus, the carbonization or thermal activation step was essential for the best performance of the materials in the removal of Allura red dye from an aqueous solution. With the results obtained in the activation method test of Fig. 8a, the adsorbent A.C. (IV) was chosen as the study material and from this moment on, all tests were performed with it.

Fig. 8b shows the results obtained in the granulometric test of the A.C. (IV) adsorbent; it was possible to observe that the particle size influenced the removal of the Allura red dye from the solution. The test with a particle size of 0.42 mm was the one that obtained the highest removal, approximately 57%, a value 10% greater than the assay with the same adsorbent in Fig. 8a, which showed that the particle size positively affected the adsorptive process. This increase in the removal may be because at smaller particle sizes, the contact area of the adsorbate is increased, as can be seen from the tendency to higher rates of dye removal with the decreasing of particle size, but for very low particle diameter values such as 0.088 mm, a sudden drop in the removal value

occurred, which can be explained by the fact that at very low diameters the saturation of the material occurs much faster due to the lower presence of active sites on the surface of the material that is extremely small. Thus, the particle size of 0.42 mm was chosen for the other adsorption tests. Analyzing Fig. 8c, it was possible to observe that the reaction medium pH influenced the adsorptive capacity of the A.C. (IV); at pH=7 the removal of Allura red dye was maximum, approximately 45%; this showed that the interaction between adsorbent and adsorbate occurred efficiently in a medium with neutral pH (~7); this was due to the electrostatic interaction between the surface charges of the material, which by PCZ analysis showed a positively charged surface, and the charges present in the solution; dyes by nature have an anionic tendency, that is, the presence of negative charges in the solution; this made the adsorption process to be favored at lower pH, as shown in Fig. 8c. Originally the pH of the dye solution was 6.81, a value very close to neutral, so an adjustment in the pH was not made necessary for further testing.

In Fig. 8d, it is clear the influence of the adsorbent concentration on the process of removal of the dye molecules from the solution; the diagram shows a clear trend of increased removal with increasing concentration; this proportionality relationship was expected, since a greater amount of adsorbent, the greater the number of active sites that can contribute to the adsorptive process. For a concentration of 2 g.L⁻¹, removal of approximately 90% was achieved; this value is very close to many works in the literature [17, 38, 71]. For concentrations greater than 5 g.L⁻¹, approximately all the dye was removed from the solution. From the technical-economic point of view, it was decided to use the concentration of 2 g.L⁻¹, since an acceptable removal was achieved with a smaller amount of adsorbent, optimizing costs for the process. With the preliminary tests done, the best parameters of each test were adopted here for all the assays in this study. Summing up, the A.C. (IV) adsorbent with a particle size of 0.42 mm and a concentration of 2 g.L⁻¹ obtained the best removal results for the Allura red dye solution at 10 mg.L⁻¹.

Batch adsorption tests

Fig. 9 shows the results for the removal of Allura red dye in the factorial design experiment, according to Table II. It was observed that assays 2, 4, and 8 were the ones that obtained the highest percentage of removal of the Allura red dye from the solutions; when observing Table II, it was possible to notice that for these tests the reaction temperatures were the highest, 40 and 44 °C; this indicated a clear influence of the reaction temperature on the adsorptive capacity of the material and this happened since low-temperature tests such as assays 1, 3, and 7, which took place at temperatures of 16 and 20 °C, were those that obtained the lowest removal values, reinforcing the hypothesis that temperature influenced the process of adsorption of dye molecules by activated carbon. The results of these assays were statistically tested to determine whether

the temperature variable affected the reaction and the results of the statistical analysis of batch tests are shown in Table VIII and Fig. 10.

It was possible to evaluate how the factors interfered with the response variable by observing the Pareto chart in Fig. 10a, where factor x (dye concentration) and factor y (reaction temperature) had a significant statistical effect on the amount of dye removed (R) in a significance level of 5%. This result can also be observed in the ANOVA table (Table VIII), where the variables reaction temperature, dye concentration², and reaction temperature² had a p-value <0.05. The residual error of the experiment was $\sqrt{3.678}=1.92$ (Table VIII). In Fig. 10b the graph between predicted and observed values is shown; it was possible to observe that the regression model satisfactorily adjusted the data, with the experimental points very close to the adjustment curve. This can be confirmed by looking at the RMSE value of the data, which was approximately 1.11, which indicated that in a global context the model had satisfactorily adjusted the experimental data, in addition to having obtained a value of $R^2_{adj}=0.9738$ (Table VIII). Fig. 10c presents the level curves obtained in the statistical analysis; the yellow-orange region showed the highest values for the variable response, R, when the value of the x-axis (dye concentration) was between 0 and 60 mg.L⁻¹ and the value of the y axis (reaction temperature) was between 35 and 45 °C; it showed that the best removal of the dye molecules occurred at higher temperatures and in different dye concentration. Moreover, Fig. 10d shows the response surface obtained for the factorial design; the graph had an upward-facing concavity that resembled a curve of a second-degree equation. As well as the level curves, the yellow-orange region showed the highest values for the quantity of Allura red dye adsorbed.

A second-order response surface model (Eq. C, Table VIII) was obtained by using the quadratic main effects model. To optimize the factorial design and maximize the

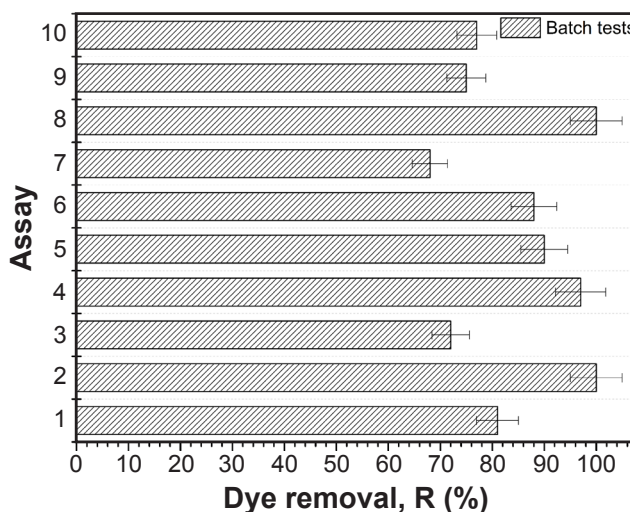


Figure 9: Dye removal of 2² factorial design assays (parameters: C₀=10 mg.L⁻¹, C_{ads}=2 g.L⁻¹, ϕ_{part} =0.42 mm, t_{rea}=12 h, V_{dye}=50 mL, T_{rea}=25 °C).

Table VIII - ANOVA results for the quadratic model of the response surface.

Source	DF	Sum of squares	Discoloration		
			Mean square	F-value	p-value
Dye concentration	1	27.48	27.48	7.473	0.052
Reaction temperature	1	995.8	995.8	270.7	0.001
Dye concentration ²	1	208.3	208.3	56.63	0.017
Reaction temperature ²	1	82.57	82.57	22.45	0.009
Concentration x Temperature	1	9.000	9.000	2.447	0.193
Residual	4	14.71	3.678		
Total	9	1265	140.6		
R ² =0.9884		R ² _{adj} =0.9738			
Fitted function		z=0.017x ² +0.0425y ² +0.0075xy-1.33x-1.659y+105.497			(C)

DF: degrees of freedom; z (%): amount of dye removed; x (mg.L⁻¹): dye concentration; y (°C): reaction temperature.

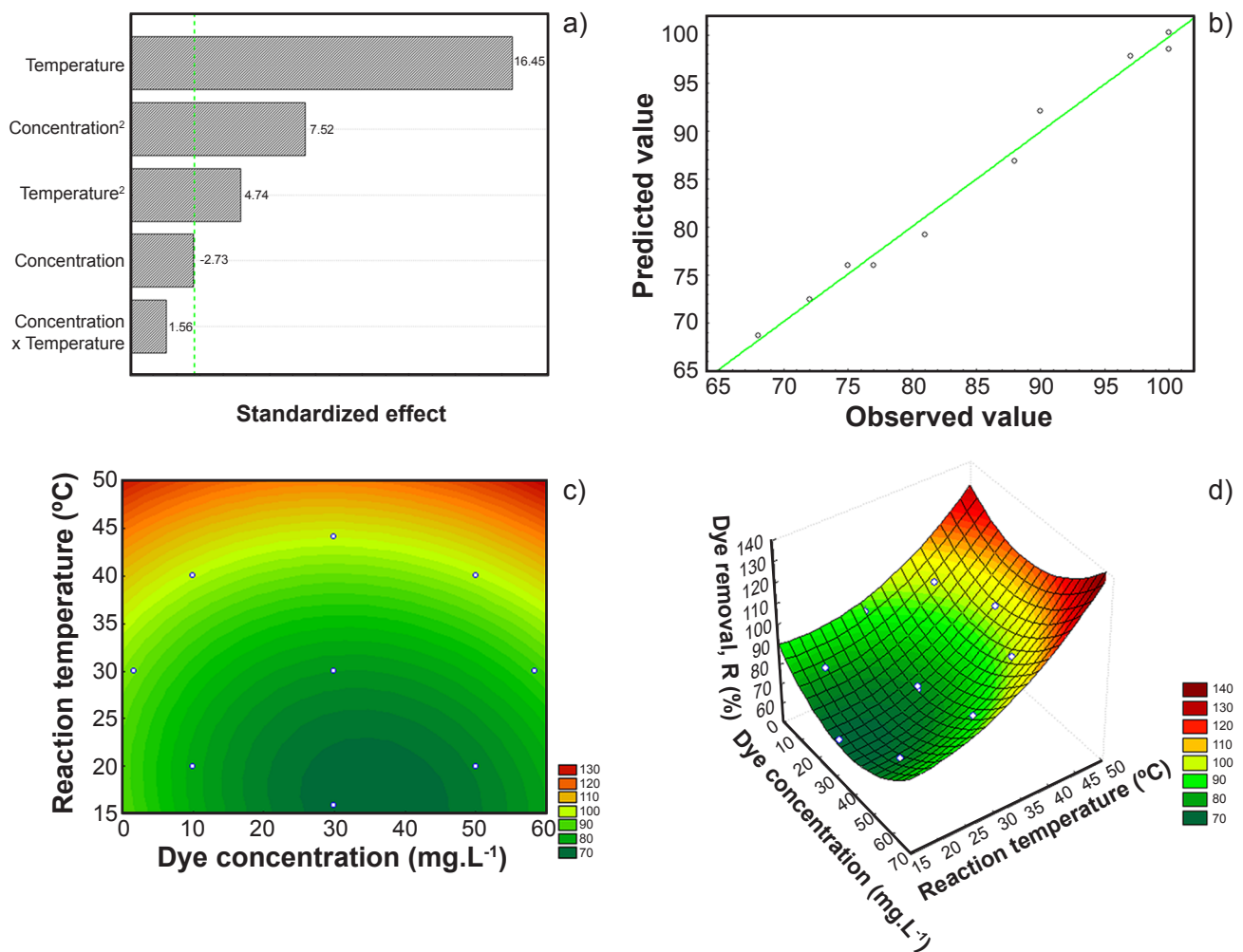


Figure 10: Results of statistical analysis of the experiment: a) Pareto chart; b) data interaction; c) level curves; and d) response surface.

value of the variable response, q_e , the model obtained was subjected to simplex method analysis to determine what is the optimum value of the factors dye concentration and

reaction temperature that generates the highest removal of Allura red dye. The calculations were performed using the solver tool in Excel. The restrictions used in the software

Table IX - Comparison of the results in the literature using adsorbent for dye removal.

Adsorbent	Mass of adsorbent (mg)	Reaction time	Adsorbate	Removal or adsorptive capacity	Ref.
Residual ash nanocomposite	100	12 h	Allura red dye	100% or 4.13 mg.g ⁻¹	This study
Zr-SBA-15 nanostructure	6.66	5.48 min	Malachite green dye	3.11 mg.g ⁻¹	[72]
			Methylene blue dye	3.56 mg.g ⁻¹	
MOF-5/Cu framework	10	2 min	Congo red dye	24.39 mg.g ⁻¹	[73]
SBA-15 zeolite	20	20 min	Cu ²⁺	9.77 mg.g ⁻¹	[74]
Ce-MOF@Fe ₃ O ₄ @AC	20	3 h	Indigo carmine dye	98%	[75]
Biosponge	100	4 h	Allura red dye	5.57 mg.g ⁻¹	[76]

were the levels imposed by the factorial design, $2 \leq \text{dye concentration} \leq 58$ and $16 \leq \text{temperature} \leq 48$ °C, and the objective was the response variable itself. The optimization results were dye concentration = 2 mg.L⁻¹ and reaction temperature = 48 °C; in these experimental conditions, the maximum value of R = 100% was achieved. The values obtained in this study were similar to those found in the literature and are shown in Table IX.

Cost analysis

The recycling of any adsorbent is important in industries once it decreases the costs of material during the wastewater treatment stage. In view of this fact, a cost analysis was carried out for the synthesis of A.C. (IV) activated carbon. The equipment was selected to meet the necessities of the synthesis; quotations were made in the state of Paraná, Brazil, and all the assumptions used were for a large industry that generates nearly 1000 kg/day of residual ash. Inputs and operating time parameters are listed in Table X. The scale-up occurred linearly from laboratory processes and thus may include some error in the amounts of materials needed to produce the adsorbents. The values in Table X are an estimation of production costs; many industries have their own methods for the activated carbon production, but these data are not available to the public. The analysis did

Table X - Assumptions for scaled-up production of activated carbon.

Input	Amount	Unit
Residual ash	1000	kg.day ⁻¹
H ₃ PO ₄	1700	kg.day ⁻¹
NaHCO ₃	1500	kg.day ⁻¹
Water usage	200	m ³ .dia ⁻¹
Electricity usage	80000	kWh
PO ₄ yield	60	%
Operational days	270	days.year ⁻¹
Active operating	20	h.day ⁻¹

not delve into characteristics such as logistical, personnel, building, and equipment costs since most of these variables depend on the country of production and it is considered that these expenses are present in the global budget of the industry, not also considering the creation of a new industry for the synthesis of this material.

Cost estimates were based on a synthesis yield of approximately 60% and an input of residual ash of 1000 kg.day⁻¹, thus the daily output of A.C. (IV) activated carbon would be around 600 kg.day⁻¹. Another assumption was that 80% of the H₃PO₄ could be recovered during the washing step, concentrated, and reused once, the same occurred for the NaHCO₃, but with a recovery rate of 20% at the end of the neutralization step. In the interest of saving costs, as well as in the bench scale synthesis, it was considered that during the carbonization stage the oven would be supplied by ambient air. Table XI shows the costs estimated for the production of A.C. (IV) activated carbon. Based on the daily production of 1000 kg of residual ash and an operational cost of 5610 USD, A.C. (IV) activated carbon would cost approximately 9.35 USD.kg⁻¹. This value is high concerning other values of activated carbon production found in the literature, such as 2.89 USD.kg⁻¹ for pecan shells activated with phosphoric acid [76] or 2.82 USD.kg⁻¹ for almond shells activated

Table XI - Production costs estimated for A.C. (IV) activated carbon.

Input	Cost
Residual ash	None
H ₃ PO ₄	2350 USD.day ⁻¹
NaHCO ₃	1450 USD.day ⁻¹
Water usage	360 USD.day ⁻¹
Electricity usage	1450 USD.day ⁻¹
Variable	Total
Operational cost	5610 USD.day ⁻¹
Production rate	600 kg.day ⁻¹
Unit production cost	9.35 USD.kg ⁻¹

with phosphoric acid [77]. However, none of these studies presented industrial applications for the obtained adsorbents and their process yield. The adsorbent in our study can treat approximately 1350 L of Allura red dye solution with 1 kg of material. If compared with a commercial 4 μm activated carbon, the price of the kg of this adsorbent is approximately 13 USD.kg⁻¹ (Synth), approximately 40% more expensive than activated carbon synthesized with H₃PO₄, reinforcing that the obtained adsorbent presents a beneficial cost for application in an industrial environment in the treatment of effluents step.

CONCLUSIONS

Nanostructured crystalline composites (activated carbon) were effectively synthesized using phosphoric acid and hydrogen peroxide as activating reagents at 400 °C. According to the characterization techniques, the adsorbent material A.C. (IV), activated with phosphoric acid and thermal treatment, had an average particle diameter of approximately 18 Å, in the range corresponding to nanometer; in addition, the material presented a crystallinity of the structure with well-defined phases such as quartz and, through the analysis of EDS, it was determined that the major elements in the composition were carbon and silicon. So, in general, it was possible to infer that a material based on nanostructured crystalline composite was synthesized and characterized with an excellent cost-benefit, being it possible to be produced at a price of 9.35 USD.kg⁻¹, a price lower than the commercial activated carbon, making it a promising candidate for application in an industrial environment. The activated carbon A.C. (IV) also had a high surface area, approximately 450 m².g⁻¹, in addition to a pH_{PZC} (pH at the point of zero charge) in the acidic range, with a highly porous and positively charged surface, which showed favorable characteristics for its use as an adsorbent for emerging pollutants. In the adsorption assays of the food dye, Allura red, the material was able to remove approximately 100% of the dye molecules from aqueous solutions, showing the possible application of this material in the treatment of effluents.

ACKNOWLEDGMENT

The authors would like to thank CNPq for the financial support during this study.

REFERENCES

- [1] K. Hui, C. Chao, S. Kot, J. Hazard. Mater. **127** (2005) 89.
- [2] F. Canpolat, K. Yilmaz, M.M. Köse, M. Sümer, M.A. Yurdusev, Cem. Concr. Res. **34** (2004) 731.
- [3] A. Rastogi, V. Kumar Paul, Environ. Res. Eng. Manag. **76** (2020) 65.
- [4] D. Zgureva, V. Stoyanova, A. Shoumkova, S. Boycheva, G. Avdeev, Crystals **10** (2020) 1064.
- [5] D. Zgureva, S. Boycheva, D. Behunová, M. Václavíková, J. Environ. Eng. **146** (2020) 4020081.
- [6] C. Baek, J. Seo, M. Choi, J. Cho, J. Ahn, K. Cho, Sustainability **10** (2018) 4854.
- [7] S. Bukhari, S. Rohani, Am. J. Environ. Sci. **13** (2017) 233.
- [8] W. Feng, Z. Wan, J. Daniels, Z. Li, G. Xiao, J. Yu, D. Xu, H. Guo, D. Zhang, E.F. May, G. Li, J. Clean. Prod. **202** (2018) 390.
- [9] J. Andrés, A. Valero, A. Medinaceli, A. Alastuey, X. Querol, N. Moreno, A. Soler, C. Ibáñez, Geol. Acta **5** (2007) 47.
- [10] S. Varandani, P. Prabhu, Int. J. Chem. **533** (2016) 313.
- [11] L.E.N. Castro, J.V.F. Santos, K.C. Fagnani, H.J. Alves, L.M.S. Colpini, J. Environ. Sci. Heal. B **54** (2019) 791.
- [12] J.F. Nure, N.T. Shibeshi, S.L. Asfaw, W. Audenaert, S.W.H. Van Hulle, Water SA **43** (2017) 470.
- [13] M.B. Ahmed, M.A. Hasan Johir, J.L. Zhou, H.H. Ngo, L.D. Nghiem, C. Richardson, M.A. Moni, M.R. Bryant, J. Clean. Prod. **225** (2019) 405.
- [14] M.J. Prauchner, F. Rodríguez-Reinoso, Microporous Mesoporous Mater. **152** (2012) 163.
- [15] T. Guimarães, A.P. de Carvalho Teixeira, A.F. de Oliveira, R.P. Lopes, New J. Chem. **44** (2020) 3310.
- [16] Ç. Öter, Ö. Selçuk Zorer, Int. J. Environ. Anal. Chem. **101** (2021) 1950.
- [17] A.H. Jawad, R. Abd Rashid, K. Ismail, S. Sabar, Desalin. Water Treat. **74** (2017) 326.
- [18] T.M. Darweesh, M.J. Ahmed, Environ. Toxicol. Pharmacol. **50** (2017) 159.
- [19] H.N. Tran, S.-J. You, H.-P. Chao, J. Environ. Manage. **188** (2017) 322.
- [20] J.F. Vivo-Vilches, A.F. Pérez-Cadenas, F.J. Maldonado-Hódar, F. Carrasco-Marín, R.P.V. Faria, A.M. Ribeiro, A.F.P. Ferreira, A.E. Rodrigues, J. Environ. Chem. Eng. **5** (2017) 1386.
- [21] S.S. Lam, M.H. Su, W.L. Nam, D.S. Thoo, C.M. Ng, R.K. Liew, P.N. Yuh Yek, N.L. Ma, D.V. Nguyen Vo, Ind. Eng. Chem. Res. **58** (2018) 695.
- [22] L. Chandana, K. Krushnamurty, D. Suryakala, C. Subrahmanyam, Mater. Today Proc. **26** (2020) 44.
- [23] M. Li, R. Xiao, Fuel Process. Technol. **186** (2019) 35.
- [24] J.A. Maciá-Agulló, B.C. Moore, D. Cazorla-Amorós, A. Linares-Solano, Carbon **42** (2004) 1367.
- [25] O. Üner, Ü. Geçgel, Y. Bayrak, Arab. J. Chem. **12** (2019) 3621.
- [26] L.E.N. de Castro, E.C. Meurer, H.J. Alves, M.A.R. dos Santos, E.C. Vasques, L.M.S. Colpini, Braz. Arch. Biol. Technol. **63** (2020) e20180573.
- [27] K.C. Fagnani, H.J. Alves, L.E.N. de Castro, S.S. Kunh, L.M.S. Colpini, J. Environ. Chem. Eng. **7** (2019) 102996.
- [28] A.L. Ahmad, S. Sumathi, B.H. Hameed, Chem. Eng. J. **118** (2006) 99.
- [29] M.A. Aboulhassan, S. Souabi, A. Yaacoubi, M. Baudu, J. Hazard. Mater. **138** (2006) 40.
- [30] V. Golob, A. Vinder, M. Simonic, Dyes Pigm. **67** (2005) 93.
- [31] M. Chowdhury, M.G. Mostafa, T.K. Biswas, A.K. Saha, Water Resour. Ind. **3** (2013) 11.

- [32] W. Qasim, A.V. Mane, *Water Resour. Ind.* **4** (2013) 1.
- [33] C. Allegre, M. Maisseu, F. Charbit, P. Moulin, J. Hazard. Mater. **116** (2004) 57.
- [34] G.L. Dotto, G. McKay, *J. Environ. Chem. Eng.* **8** (2020) 103988.
- [35] S. Barakan, V. Aghazadeh, *Environ. Sci. Pollut. Res.* **28** (2020) 2572.
- [36] N.S. Azmi, K.F.M. Yunus, *Agric. Agric. Sci. Procedia* **2** (2014) 257.
- [37] S. Gao, B.S. Villacorta, L. Ge, T.E. Rufford, Z. Zhu, *Carbon* **124** (2017) 142.
- [38] Q. Han, J. Wang, B.A. Goodman, J. Xie, Z. Liu, *Powder Technol.* **366** (2020) 239.
- [39] P. Patnukao, P. Pavasant, *Bioresour. Technol.* **99** (2008) 8540.
- [40] Y. Zhou, S. Xia, J. Zhang, Z. Zhang, S.W. Hermanowicz, *Desalin. Water Treat.* **57** (2015) 9343.
- [41] G.R. de Freitas, M.G.A. Vieira, M.G.C. da Silva, *J. Clean. Prod.* **271** (2020) 122588.
- [42] Y.K. Allo, Sudarmono, O. Togibasa, *J. Indones. Chem. Soc.* **2** (2019) 48.
- [43] A. Saravanan, P.S. Kumar, P.R. Yaashikaa, S. Karishma, S. Jeevanantham, S. Swetha, *Chemosphere* **277** (2021) 130236.
- [44] L.E.N. Castro, L.M.S. Colpini, *Eur. Food Res. Technol.* **247** (2021) 3013.
- [45] S.J. Gregg, K.S.W. Sing, *Adsorption, surface area and porosity*, Academic Press, London (1969).
- [46] G. Huang, Y. Liu, X. Wu, J. Cai, *New Carbon Mater.* **34** (2019) 247.
- [47] A. Toprak, *Biomass Convers. Biorefin.* **10** (2019) 977.
- [48] K.S.W. Sing, *Pure Appl. Chem.* **57** (1985) 603.
- [49] E.P. Barrett, L.G. Joyner, P.P. Halenda, *J. Am. Chem. Soc.* **73** (1951) 373.
- [50] A.F.M. Streit, G.C. Collazzo, S.P. Druzian, R.S. Verdi, E.L. Foletto, L.F.S. Oliveira, G.L. Dotto, *Chemosphere* **262** (2021) 128322.
- [51] Q. Liang, Y. Liu, M. Chen, L. Ma, B. Yang, L. Li, Q. Liu, *Mater. Chem. Phys.* **241** (2020) 122327.
- [52] C. Guo, L. Ding, X. Jin, H. Zhang, D. Zhang, *J. Environ. Chem. Eng.* **9** (2021) 104785.
- [53] J. Xu, L. Chen, H. Qu, Y. Jiao, J. Xie, G. Xing, *Appl. Surf. Sci.* **320** (2014) 674.
- [54] Q.-S. Liu, T. Zheng, P. Wang, L. Guo, *Ind. Crops Prod.* **31** (2010) 233.
- [55] H. Demiral, C. Güngör, *J. Clean. Prod.* **124** (2016) 103.
- [56] M. Doğan, P. Sabaz, Z. Biçici, B. Koçer Kizilduman, Y. Turhan, *J. Energy Inst.* **93** (2020) 2176.
- [57] E. Es-Sebbar, A. Jolly, Y. Benilan, A. Farooq, *J. Mol. Spectrosc.* **305** (2014) 10.
- [58] C.A. Igwegbe, J.O. Ighalo, K.K. Onyechi, O.D. Onukwuli, *Sustain. Water Resour. Manag.* **7** (2021) 39.
- [59] X. Chen, S. Jeyaseelan, N. Graham, *Waste Manag.* **22** (2002) 755.
- [60] B.S. Girgis, E. Smith, M.M. Louis, A.-N.A. El-Hendawy, *J. Anal. Appl. Pyrolysis* **86** (2009) 180.
- [61] A.E. Ogungbenro, D.V. Quang, K.A. Al-Ali, L.F. Vega, M.R.M. Abu-Zahra, *J. Environ. Chem. Eng.* **8** (2020) 104257.
- [62] JCPDS, *Powder Diffr.* **1** (1986) 66.
- [63] F. Wang, S. Gao, J. Pan, X. Li, J. Liu, *Nanomaterials* **9** (2019) 657.
- [64] S. Dong, J. Zhang, L. Gao, Y. Wang, D. Zhou, *Trans. Nonferrous Met. Soc. China* **22** (2012) 2477.
- [65] G.B. Besinella, J.E. Padilha, F.B. Scheufele, L.J. Gasparrini, C.E. Borba, H.J. Alves, *Mater. Adv.* **2** (2021) 403.
- [66] M. Aguiar, B.B. Cazula, L.M. Saragiotto Colpini, C.E. Borba, F.A. da Silva, F.B. Noronha, H.J. Alves, *Int. J. Hydrog. Energy* **44** (2019) 32003.
- [67] R.G.D. Molin Filho, L.M.S. Colpini, M.M. Ferrer, M.F. Nagano, J.M. Rosso, E.A. Volnistem, P.R. Paraíso, L.M. de Matos Jorge, *Clean Technol. Environ. Policy* **21** (2019) 1687.
- [68] B.B. Cazula, L.G. Oliveira, B. Machado, H.J. Alves, *Mater. Chem. Phys.* **266** (2021) 124553.
- [69] S.Y. Lee, H.E. Shim, J.E. Yang, Y.J. Choi, J. Jeon, *Nanomaterials* **9** (2019) 1164.
- [70] M.A. Islam, S. Sabar, A. Benhouria, W.A. Khanday, M. Asif, B.H. Hameed, *J. Taiwan Inst. Chem. Eng.* **74** (2017) 96.
- [71] M. Benadjemia, L. Millière, L. Reinert, N. Benderdouche, L. Duclaux, *Fuel Process. Technol.* **92** (2011) 1203.
- [72] F. Ramezani, R. Zare-Dorabei, *Polyhedron* **166** (2019) 153.
- [73] S.H. Mosavi, R. Zare-Dorabei, M. Bereyhi, *ChemistrySelect* **6** (2021) 4432.
- [74] S. Nazerdeylami, R. Zare-Dorabei, *Micro Nano Lett.* **14** (2019) 823.
- [75] R. Paz, H. Viltres, N.K. Gupta, C. Leyva, *J. Molec. Liq.* **337** (2021) 116578.
- [76] C. Ng, W.E. Marshall, R.M. Rao, R.R. Bansode, J.N. Losso, *Ind. Crop. Prod.* **17** (2003) 209.
- [77] C.A. Toles, W.E. Marshall, M.M. Johns, L.H. Wartelle, A. McAloon, *Bioresour. Technol.* **71** (2000) 87.
- (*Rec. 12/05/2022, Rev. 17/07/2022, Ac. 05/08/2022*)